Water Research 116 (2017) 241–253

Contents lists available at ScienceDirect

Water Research

journal homepage: www.elsevier.com/locate/watres

A mechanistic model for anaerobic phototrophs in domestic wastewater applications: Photo-anaerobic model (PAnM)

D. Puyol [a, b, c, *], E.M. Barry [a, b], T. Hülsen [a, b], D.J. Batstone [a, b]

[a] Advanced Water Management Centre, Gehrmann Building, The University of Queensland, Brisbane, Queensland 4072, Australia
[b] CRC for Water Sensitive Cities, PO Box 8000, Clayton, Victoria, 3800, Australia
[c] Group of Chemical and Environmental Engineering (GIQA), University Rey Juan Carlos, 28933 Mostoles, Madrid, Spain

ARTICLE INFO

Article history:
Received 9 December 2016
Received in revised form
7 March 2017
Accepted 8 March 2017
Available online 9 March 2017

Keywords:
Phototrophic bacteria
Resource recovery
Mechanistic modelling
Partition-release-recovery

ABSTRACT

Purple phototrophic bacteria (PPB) have been recently proposed as a key potential mechanism for accumulative biotechnologies for wastewater treatment with total nutrient recovery, low greenhouse gas emissions, and a neutral to positive energy balance. Purple phototrophic bacteria have a complex metabolism which can be regulated for process control and optimization. Since microbial processes governing PPB metabolism differ from traditional processes used for wastewater treatment (e.g., aerobic and anaerobic functional groups in ASM and ADM1), a model basis has to be developed to be used as a framework for further detailed modelling under specific situations. This work presents a mixed population phototrophic model for domestic wastewater treatment in anaerobic conditions. The model includes photoheterotrophy, which is divided into acetate consumption and other organics consumption, chemoheterotrophy (including simplified fermentation and anaerobic oxidation) and photoautotrophy (using hydrogen as an electron donor), as microbial processes, as well as hydrolysis and biomass decay as biochemical processes, and is single-biomass based. The main processes have been evaluated through targeted batch experiments, and the key kinetic and stoichiometric parameters have been determined. The process was assessed by analyzing a continuous reactor simulation scenario within a long-term wastewater treatment system in a photo-anaerobic membrane bioreactor.

1. Introduction

Wastewater treatment is shifting focus to include the capture and recovery of organics and nutrients. This requires novel technological approaches. A key approach is the use of fast growing organisms to concentrate energy, nutrients, and trace compounds into the solid phase, and hence substantially reduce reactive removal of nitrogen and organics while enabling phosphorous recovery. One option is high-rate activated sludge, which can achieve 40% nitrogen removal in the primary stage through adsorption and assimilation (Jetten et al., 1997). Algae can also be used to partition to the solid phase, but a simultaneous heterotrophic and photosynthetic mode is generally enabled by bacterial-algal associations that reduce organic substrate consumption efficiency (Muñoz and Guieysse, 2006). Purple phototrophic bacteria (PPB) present a new partitioning approach, which has been shown to completely remove nitrogen to discharge limits when sufficient organic carbon is present without the need for pure cultures, and using infra-red (IR)light only as a driver for growth (Hulsen et al., 2014).

PPB grow phototrophically rather than photosynthetically, and do not use water as an electron donor to produce oxygen and organics. They are among the most metabolically versatile organisms on earth (Hunter et al., 2008). They grow heterotrophically using a wide range of organic compounds, both in presence and absence of light (photoheterotrophy and chemoheterotrophy) (Hunter et al., 2008). However, they can also grow autotrophically by using infrared light as the energy driver for CO_2 fixation, and with inorganic electron donors such as H_2, Fe^{2+}, S^{2-} or $S_2O_3^{2-}$ (cyclic anoxygenic photosynthesis) (Overmann and Garcia-Pichel, 1998). Although they can grow in the presence of oxygen, they are extremely effective in anaerobic photoheterotrophic conditions (Gordon and McKinlay, 2014; McKinlay and Harwood, 2010). Their ability to recycle electrons during the cyclic anoxygenic photosynthesis gives them the ability to harvest and retain electrons, as well as a high energetic efficiency. This entails a much higher

* Corresponding author. Departmental Building I, Room 234, Mostoles Campus, University Rey Juan Carlos, C/ Tulipán, S/n, 28933, Mostoles, Madrid, Spain.
E-mail address: daniel.puyol@urjc.es (D. Puyol).

http://dx.doi.org/10.1016/j.watres.2017.03.022
0043-1354/

Nomenclature

ADM1	IWA Anaerobic Digestion Model #1
ASM	IWA Activated Sludge Models
$f_{ac,ch}$	Stoichiometry of acetate production in chemoheterotrophy (mgCOD $mgCOD^{-1}$)
$f_{C,B}$	Carbon content of PPB (molC $mgCOD^{-1}$)
$f_{C,si}$	Carbon content of soluble inert (molC $mgCOD^{-1}$)
$f_{C,xi}$	Carbon content of particulate inert (molC $mgCOD^{-1}$)
$f_{C,xs}$	Carbon content of biodegradable particulate (molC $mgCOD^{-1}$)
$f_{h2,a}$	Stoichiometry of hydrogen consumption in autotrophy (mgCOD $molC^{-1}$)
$f_{h2,ch}$	Stoichiometry of hydrogen production in chemoheterotrophy (mgCOD $mgCOD^{-1}$)
$f_{h2,xs}$	Stoichiometry of hydrogen production in hydrolysis (mgCOD $mgCOD^{-1}$)
$f_{IC,a}$	Stoichiometry of inorganic carbon consumption in autotrophy (molC $molC^{-1}$)
$f_{IC,ph,ac}$	Stoichiometry of inorganic carbon produced from acetate in photoheterotrophy (molC $mgCOD^{-1}$)
$f_{IC,ph,Ss}$	Stoichiometry of inorganic carbon produced from soluble fraction of substrate but acetate in photoheterotrophy (molC $mgCOD^{-1}$)
$f_{IC,xs}$	Stoichiometry of inorganic carbon production in hydrolysis (molC $mgCOD^{-1}$)
$f_{IN,xs}$	Stoichiometry of ammonia production in hydrolysis (mgN $mgCOD^{-1}$)
$f_{IP,xs}$	Stoichiometry of phosphate production in hydrolysis (mgP $mgCOD^{-1}$)
$f_{N,B}$	Nitrogen content of PPB (mgN $mgCOD^{-1}$)
$f_{N,si}$	Nitrogen content of soluble inert (mgN $mgCOD^{-1}$)
$f_{N,xi}$	Nitrogen content of particulate inert (mgN $mgCOD^{-1}$)
$f_{N,xs}$	Nitrogen content of biodegradable particulate (mgN $mgCOD^{-1}$)
$f_{P,B}$	Phosphorus content of PPB (mgP $mgCOD^{-1}$)
$f_{P,si}$	Phosphorus content of soluble inert (mgP $mgCOD^{-1}$)
$f_{P,xi}$	Phosphorus content of particulate inert (mgP $mgCOD^{-1}$)
$f_{P,xs}$	Phosphorus content of biodegradable particulate (mgP $mgCOD^{-1}$)
$f_{SAc,xs}$	Stoichiometry of acetate production in hydrolysis (mgCOD $mgCOD^{-1}$)
$f_{si,xs}$	Stoichiometry of soluble inert production in hydrolysis (mgCOD $mgCOD^{-1}$)
$f_{ss,xs}$	Stoichiometry of soluble substrate production but acetate in hydrolysis (mgCOD $mgCOD^{-1}$)
$f_{xi,xs}$	Stoichiometry of particulate inert production in hydrolysis (mgCOD $mgCOD^{-1}$)
HA	Hydrogenogenic activity ($mgCOD_{h2}$ L_{liq}^{-1} d^{-1})
HA_{max}	Maximum hydrogenogenic activity ($mgCOD_{h2}$ L_{liq}^{-1} d^{-1})
HRT	Hydraulic retention time (h)
I_{FA}	Limiting factor for free ammonia inhibition
I_{IE}	Limiting factor for light limitation
I_{IN}	Limiting factor for nitrogen limitation
I_{IP}	Limiting factor for phosphorus limitation
k_{dec}	Biomass decay first order constant (d^{-1})
k_{hyd}	Hydrolysis first order constant (d^{-1})
$K_{I,FA}$	Inhibitory constant for free ammonia (mgN L^{-1})
$k_{M,ac}$	Specific uptake rate for acetate in photoheterotrophy (mgCOD $mgCOD^{-1}$ d^{-1})
$k_{M,but}$	Specific uptake rate for butyrate in photoheterotrophy (mgCOD $mgCOD^{-1}$ d^{-1})
$k_{M,ch}$	Specific uptake rate in chemoheterotrophy (mgCOD $mgCOD^{-1}$ d^{-1})
$k_{M,et}$	Specific uptake rate for ethanol in photoheterotrophy (mgCOD $mgCOD^{-1}$ d^{-1})
$k_{M,ic}$	Specific uptake rate of IC in autotrophy (molC $mgCOD^{-1}$ d^{-1})
$k_{M,ph}$	Specific uptake rate in photoheterotrophy (mgCOD $mgCOD^{-1}$ d^{-1})
$k_{M,prop}$	Specific uptake rate of propionate in photoheterotrophy (mgCOD $mgCOD^{-1}$ d^{-1})
$K_{S,ac}$	Saturation constant for acetate in photoheterotrophy (mgCOD L^{-1})
$K_{S,but}$	Saturation constant for butyrate in photoheterotrophy (mgCOD L^{-1})
$K_{S,E}$	Saturation constant for light intensity (W m^{-2})
$K_{S,et}$	Saturation constant for ethanol in photoheterotrophy (mgCOD L^{-1})
$K_{S,h2}$	Saturation constant for H_2 consumption in autotrophy (mgCOD L^{-1})
$K_{S,IC}$	Saturation constant for inorganic carbon in autotrophy (molC L^{-1})
$K_{S,prop}$	Saturation constant for propionate in photoheterotrophy (mgCOD L^{-1})
$K_{S,s}$	Saturation constant for soluble substrate but acetate in photoheterotrophy (mgCOD L^{-1})
K_{Sin}	Saturation constant for inorganic nitrogen assimilation (mgN L^{-1})
K_{Sip}	Saturation constant for inorganic phosphorus assimilation (mgP L^{-1})
S_{ac}	Concentration of acetate (mgCOD L^{-1})
SCOD	Soluble chemical oxygen demand (mgCOD L^{-1})
S_{h2}	Concentration of hydrogen as COD (mgCOD L^{-1})
S_I	Concentration of soluble inerts (mgCOD L^{-1})
S_{IC}	Concentration of inorganic carbon (molC L^{-1})
S_{IN}	Concentration of inorganic nitrogen as ammonia (mgN L^{-1})
S_{IP}	Concentration of inorganic phosphorus as phosphate (mgP L^{-1})
SPA	Specific phototrophic activity (mgCOD $mgCOD^{-1}$ d^{-1})
SRT	Solids retention time (d^{-1})
S_s	Concentration of biodegradable soluble fraction but acetate (mgCOD L^{-1})
TCOD	Total chemical oxygen demand (mgCOD L^{-1})
TIC	Total inorganic carbon (molC L^{-1})
TKN	Total Kjeldahl Nitrogen (mgN L^{-1})
TP	Total phosphorus (mgP L^{-1})
TSS	Total suspended solids (mg L^{-1})
VFA	Volatile fatty acids (mgCOD L^{-1})
VLR	Volumetric loading rate (mgCOD L^{-1} d^{-1})
VSS	Volatile suspended solids (mg L^{-1})
X_I	Concentration of particulate inerts (mgCOD L^{-1})
X_{PB}	Concentration of PPB biomass (mgCOD L^{-1})
X_S	Concentration of organic biodegradable particulate (mgCOD L^{-1})
Y_{ac}	Biomass yield on acetate in photoheterotrophy (mgCOD $mgCOD^{-1}$)
Y_{but}	Biomass yield on butyrate in photoheterotrophy (mgCOD $mgCOD^{-1}$)
Y_{et}	Biomass yield on ethanol in photoheterotrophy (mgCOD $mgCOD^{-1}$)
$Y_{PB,a}$	Biomass yield in autotrophy (mgCOD $molC^{-1}$)
$Y_{PB,ch}$	Biomass yield in chemoheterotrophy (mgCOD $mgCOD^{-1}$)
$Y_{PB,ph}$	Biomass yield in photoheterotrophy (mgCOD $mgCOD^{-1}$)
Y_{prop}	Biomass yield on propionate in photoheterotrophy (mgCOD $mgCOD^{-1}$)

biomass yield on organic substrates than traditional aerobic biomass (near 1 vs 0.6 gCOD $dCOD^{-1}$) (Hulsen et al., 2014). They can even accumulate electrons in the form of reduced cofactors which enable the disposal of electrons. This can be done through two main strategies: (i) ATP-driven hydrogen production by ferredoxin oxidation in the hydrogenase/nitrogenase system at the end of the electron transport chain (ETC), and (ii) the increase of assimilative growth by re-fixation of CO_2 via the Calvin Cycle produced during heterotrophic metabolism (McKinlay and Harwood, 2010). These metabolic features give them the possibility of growing and outcompeting other heterotrophic microorganisms where light is present, including in low to medium strength wastewater systems with short hydraulic retention times (HRT) (Hulsen et al., 2014).

PPB have a number of additional metabolic functions useful in wastewater treatment systems. They are able to accumulate polymers such as poly-phosphate (poly-P) (Liang et al., 2010), polysaccharides (Klein et al., 1991), poly-β hydroxybutyrate (PHB) (Melnicki et al., 2009) and other poly-3(hydroxyalkanoates) (PHA) (Brandl et al., 1991). Under an excess of organics and available energy, and in the absence of mineral nitrogen, they generate hydrogen and fix nitrogen as ammonia (Basak and Das, 2007).

PPB have been assessed for wastewater treatment, particularly for processing swine (Kim et al., 2004), latex rubber-sheet (Kantachote et al., 2005), tofu (Zhu et al., 1999), and sugar refinery wastewaters (Yetis et al., 2000). However, most of these studies were focused on hydrogen production rather than organics removal or nutrient recovery (Fang et al., 2005; Lee et al., 2010; Tao et al., 2008). They have also been applied to domestic wastewater (DWW) in batch and continuous operation to remove nitrogen to discharge limits (Hulsen et al., 2014; Hülsen et al., 2016b). This process enables a single-step treatment of wastewater with HRT and effluent qualities similar to those of activated sludge processes without destroying nitrogen and phosphorus.

Modelling is used to design, benchmark, and analyze wastewater treatment systems, with the IWA Activate Sludge Model (ASM) family models being the most widely used for conventional activated sludge processes (Henze et al., 2000). The IWA anaerobic digestion model no. 1 (ADM-1) is the analogous model for domestic and industrial anaerobic systems (Batstone et al., 2002). The IWA Models, and wastewater modelling in general has generally applied first order hydrolysis for solids transformation (including decay), Monod kinetic function for uptake kinetics and inverse Monod kinetic function (non-competitive) for inhibition functions, with a COD basis for organics and molar basis for inorganic compounds. Development of new technologies such as PPB requires development of a similar mechanistic model to allow process control, design, and system analysis in upscaled applications.

There are complex metabolic models based on PPB metabolism primarily focused on the electron transport chain (Golomysova et al., 2010; Klamt et al., 2002). Due to their complexity, these models are motivated more by a need for a mechanistic understanding of the underlying process rather than field applications. These models are therefore unsuitable for a wastewater model. In particular, they include components which can't be measured readily, making validation difficult. They also lack capability outside the core application area. There has also been work done on modelling PPB to describe hydrogen production (Eroglu, 2008; Gadhamshetty et al., 2008; Obeid et al., 2009). In contrast, due to the domestic wastewater matrix, the key growth modes are photoheterotrophy (principal) as well as chemoheterotrophy and photoautotrophy. Biochemical processes relevant to complex substrates such as solids hydrolysis and biomass decay must be considered as well. Therefore, this work aims to propose a mechanistic model for mixed culture PPB as a partition agent in DWW treatment with adaptability to treatment of industrial wastewaters.

2. Materials and methods

2.1. Model description

The model was developed to be unit-compatible with the IWA ASM and ADM series (Batstone et al., 2002; Henze et al., 2000). Therefore, units of mgCOD L^{-1} (or gCOD m^{-3}) for both soluble and particulate organics were chosen. Nutrient units are in mgN L^{-1} and mgP L^{-1}, respectively, with inorganic carbon (IC, HCO_3^-) in molC L^{-1}.

Monod kinetics is uniformly applied for biological growth processes, with first order kinetics for hydrolysis and decay. Monod or non-competitive inhibition has been applied for limiting or inhibitory expressions respectively. Due to a lack of functional differentiation within the PPB clade, and limited evidence to the contrary, only one biomass component has been selected (PPB) (Hülsen et al., 2016b). Other biological groups present in ASM and ADM1 models (e.g., hydrogen utilizing methanogens, denitrifiers or fermentative bacteria) could be readily included. As in the ASM/ADM models S_i is used for soluble compounds, and X_i for particulate compounds, where subscript i denotes the compound.

The model does not currently include poly-P or other polymer accumulation, since this occurs mainly in static (not growing) mode, where PPB can derive energy to stock resources for further usage in growing conditions (Hiraishi et al., 1991; Liang et al., 2010). Likewise, nitrification/denitrification processes are not included, since they can only occur in, or in combination with aerobic conditions where ammonia can be oxidized to nitrite or nitrate. Therefore, N and P are removed by assimilative growth only.

In the presence of organic substrates and IR light, photoheterotrophy through the tri-carboxylic acid (TCA) cycle is assumed to dominate. Two major mechanisms of electron disposal by PPB are considered. Firstly, the production of CO_2 (S_{IC}) is a key feature of PPB biomass under growth conditions (McKinlay and Harwood, 2010) and is important for closing the C balance. The oxidation state of the organic compound determines if the biomass fixes CO_2 for substrate uptake and electron balance (in the case of reduced substrates such as propionate, butyrate or valerate), or the uptake produces CO_2 (in the case of oxidized substrates such as acetate or succinate) (McKinlay and Harwood, 2011). In the latter case, the biomass disposes of excess of electrons by re-fixing the CO_2 produced in the TCA cycle. As a consequence, there is usually limited consumption or production of CO_2 in domestic wastewater. A theoretical explanation of this mechanism is explained in Supplementary Information (SI). The other major mechanism of electron disposal by PPB is H_2 production via the nitrogenase complex. In static growth mode, the PPB biomass is able to use the excess of electrons for redox balance at the end of the ETC. The ferredoxin complex is the carrier for this process, but the biomass needs energy in the form of ATP (Golomysova et al., 2010). However, this process is inhibited in presence of NH_4^+, a strong inhibitor of the nitrogenase activity (Rodionov et al., 1986). Indeed, H_2 production is inhibited in a DWW fed situation due to (i) presence of ammonium and (ii) disposing of electrons by CO_2 re-fixation which promotes growth (see SI for more details). Therefore, it can be deduced that CO_2 production and re-fixation into the Calvin Cycle is the major electron sink in PPB metabolism. In the absence of organic substrates, autotrophic growth is the sole growth mode, using reduced inorganic compounds other than water as electron donor (anoxygenic photosynthesis). In the interest of model simplification and considering domestic wastewater contains generally low sulfur levels, the sulfur cycle has been omitted. It is however possible to add sulfate reduction into the model with subsequent sulfide utilization as an electron donor for autotrophic PPB growth. This would require the addition of another biomass component (PPB cannot perform sulfate reduction). PPB can

perform chemoheterotrophy at a lower rate, providing H_2 (S_{h2}) for photoautotrophy (Golomysova et al., 2010).

Transforming these mechanisms to a model enables the following key processes (Fig. 1):

(i) *Photoheterotrophy on acetate (S_{ac}) (acetate uptake):* This involves acetate assimilation by PPB in the presence of infra-red radiation. Acetate is represented as a separate state due to differences observed during batch tests. Due to an imbalance in substrate-biomass carbon oxidation state, this process results in production of CO_2.

(ii) *Photoheterotrophy on other organics (S_S) (photoheterotrophic uptake):* These include all soluble organics that PPB can assimilate for growth in the presence of infra-red radiation. Compounds include VFAs excluding acetate, alcohols, and some sugars. These have been lumped into a single soluble substrate. Similar to (i) this results in the uptake of CO_2.

(iii) *Chemoheterotrophy (chemoheterotrophic uptake):* This process involves the assimilative consumption of any organic in dark conditions that can be metabolized through either fermentation or anaerobic oxidation processes. All these processes have been joined as one process for a sake of simplicity. This process involves H_2 and acetate as end products. Acetate is not further oxidized through chemoheterotrophy due to a lack or very limited terminal electron acceptors such as Fe(III) and sulfate (Finneran et al., 2003).

(iv) *Photoautotrophy (autotrophic uptake):* This process involves assimilative CO_2 fixation by PPB in the presence of infra-red radiation using H_2 as the electron donor. Other electron donors such as Fe^{2+}, S^{2-} and $S_2O_3^-$ have been omitted but could be included.

(v) *PPB cell death (decay)*: This process involves the deactivation of PPB by cell death. Ammonium, phosphate and inorganic carbon are released and the biomass is converted into biodegradable organic particulates (X_S) and particulate inerts (X_I).

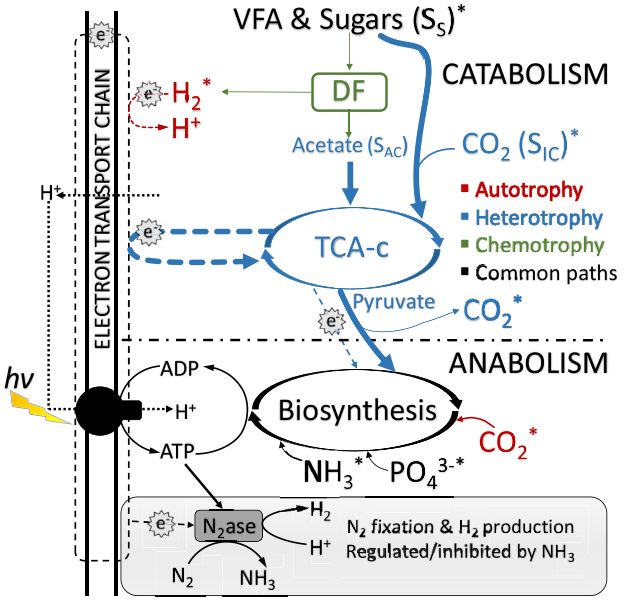

Fig. 1. Schematic summary of PPB metabolism under domestic wastewater treatment. Key: N2ase: Nitrogenase complex. TCA-c: Tri-carboxylic acid cycle. DF: Dark fermentation. VFA: volatile fatty acids. e^-: electrons. Dash: electron cycles. Dot: proton pumps. *: Model components.

(vi) *Hydrolysis and particulate fermentation (hydrolysis):* The decomposition of biodegradable particulates into organics (S_{ac} and S_S), ammonium, phosphate, hydrogen and inorganic carbon is addressed as a sole process for simplicity. Both soluble and particulate inerts are also products of this process. A breakdown of particulate fermentation could be incorporated into the model *e.g.* for processes with long solids retention times (SRT).

The model is presented in Petersen matrix notation in Table 1. Kinetic parameters were generally obtained from the batch experiments, or from the literature in specific cases as described below. The saturation constant for hydrogen consumption by photoautotrophic process ($K_{S,h2}$), light limitation ($K_{S,E}$) and inhibition by free ammonia ($K_{I,FA}$) were set arbitrarily low since affinity is high (Chen et al., 2008; Uyar et al., 2007). Competitive inhibition between S_{ac} and S_S in photoheterotrophic metabolism has been included by using a parameter-less switch function as in the case of the ADM1. This is supported by our experiments (data not shown). Stoichiometry was determined by both theoretical calculations from literature, and experimentally. The model is balanced over COD, C, N and P. Carbonates (S_{IC}), inorganic nitrogen (S_{IN}) and phosphates (S_{IP}) have been used for closing C, N and P balances, respectively.

A basic ideal activity pH model has been included as for the ADM1 (Batstone et al., 2002), with inclusion of the phosphate ($H_2PO_4^-/HPO_4^{2-}$) acid-base pair, and with no ion pairing. This provides essential representation for domestic wastewater strength, but should be extended to the strong acids and bases (H_3PO_4, PO_4^{-3}, CO_3^{2-}) where precipitation occurs, pH extremes, or higher strength is important, or where plant-wide modelling is applied as discussed in Batstone et al. (2012). Acid-base equations are formulated into the charge balance, which is solved for the single unknown of hydrogen ion (S_H) using the Matlab command fzero. Temperature is currently fixed to 25 °C, but can be incorporated via the van't Hoff equations as for Batstone et al. (2002). Background cations (S_{cat}) was set at 0.003 M to account for strong cations coupled with input bicarbonate (setting input pH to 6), but an alternative implementation where it was linked to bicarbonate was also evaluated. Acetate (S_{ac}) was added as glacial acetic acid. If sodium acetate were added instead, additional cations (S_{cat}) would need to be included. Non-VFA organics (S_S) was given an acidic fraction of 50%, assuming it to be propionic acid, with the remainder being alcohols and sugars.

Additional details concerning model development and implementation can be found in the supplementary information (SI) and codes can be found on the UQ repository (http://espace.library.uq.edu.au/view/UQ:412280). SI1 includes the description of model components, full kinetic parameters and stoichiometric coefficients. The determination and calibration of stoichiometry is included in SI2, and SI4 contains the full list of model equations.

2.1.1. Model integration with ASM-family models and ADM1

Soluble organic compounds can be readily transformed into ASM organic substrate (where $S_s\_ASM = S_{ac} + S_s\_PAnM$). Organic particulates in the PAnM correspond to the X_S in the ASM. For the ADM1 integration, an interface can be used following Nopens et al. (2009), with units generally being compatible. Mechanisms for organic biodegradable particulates to engage with the ADM1 can be approximated as follows: $X_{PPB} \rightarrow (aX_{ch} + bX_{li} + cX_{pr} + dX_I)$, where a, b, c and d are the carbohydrate, lipid, protein and inerts content of the PPB biomass as for Nopens et al. (2009). As PPB have different composition of other feedstocks, it is necessary to identify a, b, c and d parameters through nitrogen content and COD:mass ratios as done in Nopens et al. (2009). Generally, N content of PPB biomass is

Table 1
Petersen matrix of the PAM-1 model for domestic wastewater treatment by PPB.

Component (C) →	i	1	2	3	4	5	6	7	8	9	10
j	Process↓	S_S	S_{ac}	S_{IC}	S_{h2}	S_{IN}	S_{IP}	S_I	X_{PB}	X_S	X_I
1	Hydrolysis/ fermentation	$f_{ss,xs}$	$f_{sac,xs}$	$f_{IC,xs}$	$f_{h2,xs}$	$f_{IN,xs}$	$f_{IP,xs}$	$f_{si,xs}$	0	−1	$f_{xi,xS}$
2	Acetate uptake	0	−1	$f_{IC,ph,ac}$	0	$-f_{N,B}Y_{PB,ph}$	$-f_{P,B}Y_{PB,ph}$	0	$Y_{PB,ph}$	0	0
3	Photoheterotrophic uptake	−1	0	$-f_{IC,ph}$,S_s	0	$-f_{N,B}Y_{PB,ph}$	$-f_{P,B}Y_{PB,ph}$	0	$Y_{PB,ph}$	0	0
4	Chemoheterotrophic uptake	−1	$(1-Y_{PB,ch})$ $f_{ac,ch}$	0	$(1-Y_{PB,ch})$ $f_{h2,ch}$	$-f_{N,B}Y_{PB,ch}$	$-f_{P,B}Y_{PB,ch}$	0	$Y_{PB,ch}$	0	0
5	Autotrophic uptake	0	0	$-f_{IC,a}$	$-f_{h2,a}$	$-f_{N,B}Y_{PB,a}$	$-f_{P,B}Y_{PB,a}$	0	$Y_{PB,a}$	0	0
6	Decay of XPB	0	0	$-\sum_{i=8-9} Ci \times f_{C,i}$	0	$-\sum_{i=8-9} Ci \times f_{N,i}$	$-\sum_{i=8-9} Ci \times f_{P,i}$	0	−1	1	0
		Soluble substrate (mgCOD L^{-1})	Acetate (mgCOD L^{-1})	Inorganic carbon (molC_HCO3 L^{-1})	H^2 (mgCOD L^{-1})	Inorganic nitrogen (mgN_NH_4 L^{-1})	Inorganic phosphorous (mgP_PO_4 L^{-1})	Soluble inert (mgCOD L^{-1})	Phototrophic biomass (mgCOD L^{-1})	Biodegradable particulate (mgCOD L^{-1})	Particulate inert (mgCOD L^{-1})

Rate equations:

j1: $\rho_{HYD} = k_{HYD}X_S$

j2: $\rho_{ACT} = k_{M,ac}X_{PB}\left(\frac{S_{ac}}{K_{S,ac}+S_{ac}}\right)I_{FA}I_{IN}I_{IP}I_E I_{C\_S}$

j3: $\rho_{PHT} = k_{M,ph}X_{PB}\left(\frac{S_s}{K_{S,s}+S_s}\right)I_{FA}I_{IN}I_{IP}I_E I_{C\_ac}$

j4: $\rho_{AUT} = k_{M,IC}X_{PB}\left(\frac{S_{IC}}{K_{S,IC}+S_{IC}}\right)I_{FA}I_{IN}I_{IP}I_E$

j5: $\rho_{CHE} = k_{M,ch}X_{PB}\left(\frac{S_B}{K_{S,B}+S_B}\right)I_{FA}I_{IN}I_{IP}$

j6: $\rho_{DEC} = k_{DEC}X_{PB}$

Limiting factors:

Competitive inhibition: $I_{C\_S} = \frac{S_{ac}}{S_{ac}+S_S}$ $I_{C\_ac} = \frac{S_S}{S_S+S_{ac}}$

N: $I_{IN} = \left(\frac{S_{IN}}{K_{S,IN}+S_{IN}}\right)$ P: $I_{IP} = \left(\frac{S_{IP}}{K_{S,IP}+S_{IP}}\right)$ Free Ammonia: $I_{FA} = \left(\frac{K_{I,FA}}{K_{I,FA}+S_{NH3}}\right)$ Light: $I_E = \left(\frac{S_E}{K_{S,E}+S_E}\right)$

significantly higher than typical waste sludge (Hulsen et al., 2014), and this increases *c*. Both soluble and particulate inerts have the same meaning than their respective counterparts in the ASM and ADM1 models.

Inorganic nitrogen can be directly transformed into ASM inorganic nitrogen since $S_{IN\_PAnM} = S_{nh} + S_{no}$ (in mgN L^{-1}). Inorganic nitrogen in the PAnM (ammonium) has the same meaning that in the ADM1. However, total nitrogen can be integrated into ADM1 parameters by following the lump–delump approach of the Copp interface (Copp et al., 2003). Inorganic phosphorus in the PAnM has the same meaning that S_{IP} in the ADM1 and S_{PO4} in the ASM2d. The inorganic carbon in the PAnM has the same meaning as in the ADM1. Alkalinity from ASM models can be transformed into S_{IC} as in the case of the ASM1/ADM1 interface (Nopens et al., 2009).

2.2. Batch experiments

Batch experiments were done to identify parameters based on the developed model. The inoculum was sourced from a lab-scale continuous photo-anaerobic membrane bioreactor (PAnMBR) described by (Hülsen et al., 2016b) operated over 300 d. Domestic wastewater was collected from the Taringa wastewater lift station (Brisbane, Australia) with an average strength of 572 mgCOD L^{-1} and soluble COD of 241 mgCOD L^{-1}, 63 mgN L^{-1}, and 9 mgP L^{-1}.

Where wastewater was not the medium, synthetic Ormerod medium was used at pH 7.5 as described previously (Hulsen et al., 2014).

Metabolic growth batch tests: All batch tests were done in 100 mL working volumes (160 mL serum flasks) in triplicate, inoculated from the PAnMBR reactor. The headspace was flushed with N_2 and experiments were carried out at 20 °C in an orbital shaker at 150 rpm (Edwards Instrument Company). The array of flasks was irradiated with 150W lamps using UV-VIS absorbing foil as described elsewhere (Hulsen et al., 2014). All experiments were accompanied by blank samples with no substrate, and by positive and negative controls where necessary. A summary is provided in Table 2.

Hydrolysis and biomass decay: The inoculum (0.5 L) was collected as per the above method (2.1 g VSS L^{-1}). The biomass was centrifuged in 50 mL Falcon tubes and the pellet resuspended again in NaCl 0.2 M three times. Biomass was then placed in 0.5 L of NaCl 0.2 M and was divided into two 0.25 L Schott bottles, which were subsequently flushed with N_2 and magnetically stirred at 200 rpm. The bottles were operated for 30 d.

One of the bottles was covered with aluminum foil to avoid phototrophic activity, and was used for the hydrolysis analysis. Liquid sampling was performed twice a week to analyze volatile fatty acids (VFAs), NH_4-N, PO_4-P, total inorganic carbon (TIC) and pH. Headspace was analyzed for CH_4, H_2 and CO_2. TSS/VSS, TKN and TP was analyzed every 7 d.

The other bottle was illuminated as indicated above without feed, and biomass samples were taken every 7 d to assess activity (determining decay coefficient). Activity tests were done as above with 100 mgCOD L^{-1} of acetate and 10 mg NH_4-N L^{-1}.

Calculation of Specific Phototrophic Activities (SPA). Non-linear parameter estimation is generally used to determine parameters as described in 2.4.2, but specific phototrophic activity was also determined by linear regression of substrate concentration over a minimum of four points through the region of maximum consumption divided by biomass concentration.

2.3. Analytical methods

Total COD (TCOD) and soluble COD (SCOD) were determined by COD cell tests (Merck, 1.14541.0001, Darmstadt, Germany). Dissolved NH_4 -N, NO_2-N and PO_4-P were determined by a QuikChem8000 Flow Injection Analyzer (FIA) (Hach Company, Loveland, USA). Temperature and pH were measured using an Oakton pH 11 Series (Vernon Hill, IL, USA). TSS and VSS were determined by filtration according to standard methods where TSS were calculated after drying the sample in an oven at 105 ± 2 °C and VSS were calculated after burning it in a furnace at 550 ± 5 °C (APHA., 1998). Illuminance (W m^{-2}) was measured with an IR light sensor (PAS Port™, Roseville, CA, USA). VFA samples were analyzed by gas chromatography (Agilent Technologies 7890A GC System, Santa Clara, CA, USA) equipped with a flame ionization detector (GC/FID) and a polar capillary column (DB-FFAP). Gas samples were analyzed by GC (2014 Shimadzu, Kyoto, Japan) with thermal coupled detector (TCD) (Tait et al., 2009). TKN and TP were determined using sulfuric acid, potassium sulfate and copper sulfate catalyst in a block digester (Lachat BD-46, Hach Company, Loveland, CO, USA) (Patton and Truitt, 1992). TIC was analyzed by using a total organic carbon (TOC) analyzer (Shimadzu TOC-L CSH TOC Analyzer with TNM-L TN unit) coupled to a near infrared detector (NIRD) for measuring the CO_2. All soluble constituents were determined after filtering with a 0.45 μm membrane filter (Millipore, Millex®-HP, Merck Group, Darmstadt, Germany).

2.4. Data analysis

2.4.1. Data handling

Biomass concentration was calculated in g VSS L^{-1}, and it was further transformed into COD by using the COD relationship calculated from the biomass equation $CH_{1.8}O_{0.38}N_{0.18}$ (McKinlay and

Table 2
Batch conditions of the different metabolic tests.

Mechanism	Medium	Buffer system[a]	COD/N/P (C/N/P)[c]	C source (mgCOD L^{-1})	Electron donor (mg L^{-1})	Electron acceptor	Positive control	Negative control
Photoheterotrophy	Ormerod	HEPES	100/10/2	Acetate (130), propionate, butyrate, ethanol (100)	Organic	CO_2	Adding 1 g $NaHCO_3$	–
Nitrogen limitation	Ormerod	HEPES	100/1.4/2	Acetate (130)	Organic	CO_2	No N limitation	–
Phosphorus limitation	Ormerod	HEPES	100/10/0.15	Acetate (130)	Organic	CO_2	No P limitation	–
Photoautotrophy	Ormerod	Phosphate	(100/20/∞)	$NaHCO_3$ (0.012)[b]	Na_2S (300)	CO_2	–	No Na_2S
Chemoheterotrophy (dark)	Ormerod	HEPES	100/10/2	Ethanol (60), Acetate (130)	Organic	Acetate	With light	–
Inhibition of H_2 production	DWW	–	100/12/4	DWW (278)	Organic	CO_2	–	Acetate (600)
	Ormerod	Phosphate	100/15/∞	Acetate (600)	Organic	CO_2	–	N limitation (1/10)

[a] Buffer systems: HEPES (5.9 g L^{-1}), Phosphate (0.9 g K_2HPO_4 + 0.66 g KH_2PO_4).
[b] molC L^{-1}.
[c] ∞ means in high excess due to buffering.

Harwood, 2010) (1 g biomass expressed as VSS = 1.78 gCOD).

Biomass yields (Y) were calculated accounting for the initial and final biomass concentration (in g VSS L^{-1}) based on substrate consumption. Biomass concentration was further transformed into COD and then yields are expressed as $mgCOD_{biomass}$ $mgCOD^{-1}$.

2.4.2. Statistical analyses and uncertainty assessment

Good measurement practice was applied to minimize uncertainty. Where measurements were outside the calibration range, these were repeated by diluting the sample. Internal or external standards were used for all measurements. Calibration of equipment was performed at least once per week.

All parameters were estimated from triplicate batch/measurements by minimization of residual sum of squares (J = RSS). Parameter uncertainty was determined using two-tailed t-tests calculated from standard error in parameter value, obtained from the Fisher information matrix. Where parameter optimization problems involve multiple parameters (k_M, K_S), parameter uncertainty surface ($J = J_{crit}$) has also been assessed as described in (Batstone et al., 2003). Confidence intervals (at 95%) were also calculated based on two-tailed t-tests from parameter standard error, as above, and used for statistical representative comparisons. Error bars in experimental data represent 95% confidence intervals in mean based on a two-tailed t-test (5% significance threshold). Uncertainty of the slope for the analysis of SPA was determined by error in slope from linear regression in Microsoft Excel 2013 (using the Regression tool in the Data Analysis toolpack). Standard error in slope was subsequently converted into 95% confidence interval (two-tailed t-test). All statistical analyses were done with a 5% significance threshold.

2.5. Simulation of a continuous PAnMBR

The resulting kinetic expressions were used in the development of a continuous PAnMBR model. As previously demonstrated, the concentration of the bioavailable SCOD in medium strength domestic wastewater is insufficient for the system to achieve total nitrogen and total phosphorous discharge limits (Hülsen et al., 2016b). To achieve full removal, additional SCOD is required.

The goals of the simulation were the following: a) to highlight the requirement of additional SCOD to achieve total nutrient removal, and b) to demonstrate that the inclusion of a primary clarifier can lead to an organic sludge enriched in PPB biomass. Dynamic influent data was simulated according to the influent generator model developed by Gernaey et al. (2011), and adapted to the typical concentrations of primary influent reported by Hulsen et al., 2014). Based on the average influent characteristics and an HRT of 12 h, volumetric loading rate (VLR) of 1400 ± 12 mgCOD L^{-1} d^{-1} and a solid retention time (SRT) of 3 d, a reactor volume of 70 m^3 was applied. An ideal primary clarifier was included, with a solids removal efficiency of 60% ± 3% (Tchobanoglous et al., 2002).

Simulation and subsequent data processing were done in Matlab (MATLAB R2015a, The MathWorks Inc., Natick, MA). As the system of equations is stiff, the system of ordinary differential equations was solved by ODE15s. The case was simulated for 609 days with 3 stages of differing SCOD concentrations. The dynamic influent after settling was applied directly during Stage I until day 300. During Stage II (days 300–450), acetate was added to the optimum COD/N/P ratio of 100/7.1/1.8 (optimum ratio calculation reported in SI, section S6) based on the limiting nutrient (N or P). During Stage III, acetate addition was ceased. This was to assess process response to a sudden change, and to demonstrate that the system requires wastewater with a specific COD/N/P ratio. State equations were implemented in a fixed volume, completely mixed membrane bioreactor.

The results from the simulation were balanced over COD, N, P and C, and have been included in the SI.

The Matlab function and run files, along with their supporting datasets, have been uploaded to http://espace.library.uq.edu.au/view/UQ:412280.

3. Results

The sludge used for all the experiments came from a lab-scale PAnMBR (Hülsen et al., 2016b). Most of the microorganisms are related with *α-proteobacteria,* PPB accounting for more than 70% of the total gene copies detected by the pyrosequencing technique. The genus *Rhodobacter* ssp. is the most abundant, representing more than 60% of the microbiota (Hülsen et al., 2016b). The presence of photosynthetic organisms such as microalgae and cyanobacteria accounts for less than 1% of total gene copies. Therefore, the photo-biomass can be considered as PPB-dominated.

3.1. Growth processes

Photoheterotrophy was assessed with VFAs and ethanol as substrate (Fig. 2a). All substrates were completely consumed during the experiment, and overall yields were similar in all cases, with an average biomass yield of 1.13 ± 0.21 $mgCOD_{biomass}$ $mgCOD^{-1}$. More details are provided in the SI. As can be seen in Fig. 2b, uptake rates of substrates excluding acetate were similar, with a k_M of 1.3 ± 0.1 (mgCOD $mgCOD^{-1}$ d^{-1}), and undetectable K_S. Acetate had a significantly higher k_M (2.4 ± 0.2 mgCOD $mgCOD^{-1}d^{-1}$) and detectable, albeit low, K_S of 20 ± 4 mgCOD L^{-1}. This essentially means that growth (uptake) is faster on acetate, but with a lower affinity such that acetate uptake is faster at the beginning of the batch, but slower at the end.

The analysis of chemoheterotrophic metabolism by PPB was conducted by using acetate and ethanol as substrates in dark conditions (Fig. 2c). PPB biomass was much less effective in dark conditions compared with light conditions (biomass yield 0.5 vs 1.1 $mgCOD_{biomass}$ $mgCOD^{-1}$ in dark and light conditions, respectively). Biomass yield in dark conditions is relatively high compared to typical values reported in literature for dark fermentation and anaerobic oxidation processes, which are rarely greater than 0.2 $mgCOD_{biomass}$ $mgCOD^{-1}$ (Batstone et al., 2002). The occurrence of energy storage (particularly poly-P) may have a significant role here due to batch operation (Liang et al., 2010). A continuous system may differ from this depending on the illumination cycle. One with illumination in excess (operating with photo-heterotrophic growth only) is not influenced by dark anaerobic fermentation. Where the illumination-non-illumination is separated by a cycle on the order of days (or less), either in time or space, through reactor configuration or a day-night illumination cycle the response is likely to be similar to the batch response here (since the time scale is similar). However, where there are longer dark periods, stored energy may be depleted, and this requires further investigation, since there is no supporting literature. This may require inclusion of energy storage polymers, including poly-P, and possibly PHA as well as consideration of methanogenic processes that occur when photoheterotrophs can no longer effectively remove substrate.

The maximum uptake rate under dark conditions is approximately half that of photoheterotrophy (Fig. 2d), though with again, extremely low K_S values. While chemotrophic growth is not dominant under photoheterotrophic conditions, it can be very important to consider in reactor design (e.g., where there is insufficient light), and also for balancing COD, C, N and P.

Analysis of photoautotrophy was done with $NaHCO_3$ as C source and Na_2S as electron donor in 5-fold stoichiometric excess (see Table 2) (Fig. 2e). The biomass had a yield of 36,000 $mgCOD_{biomass}$

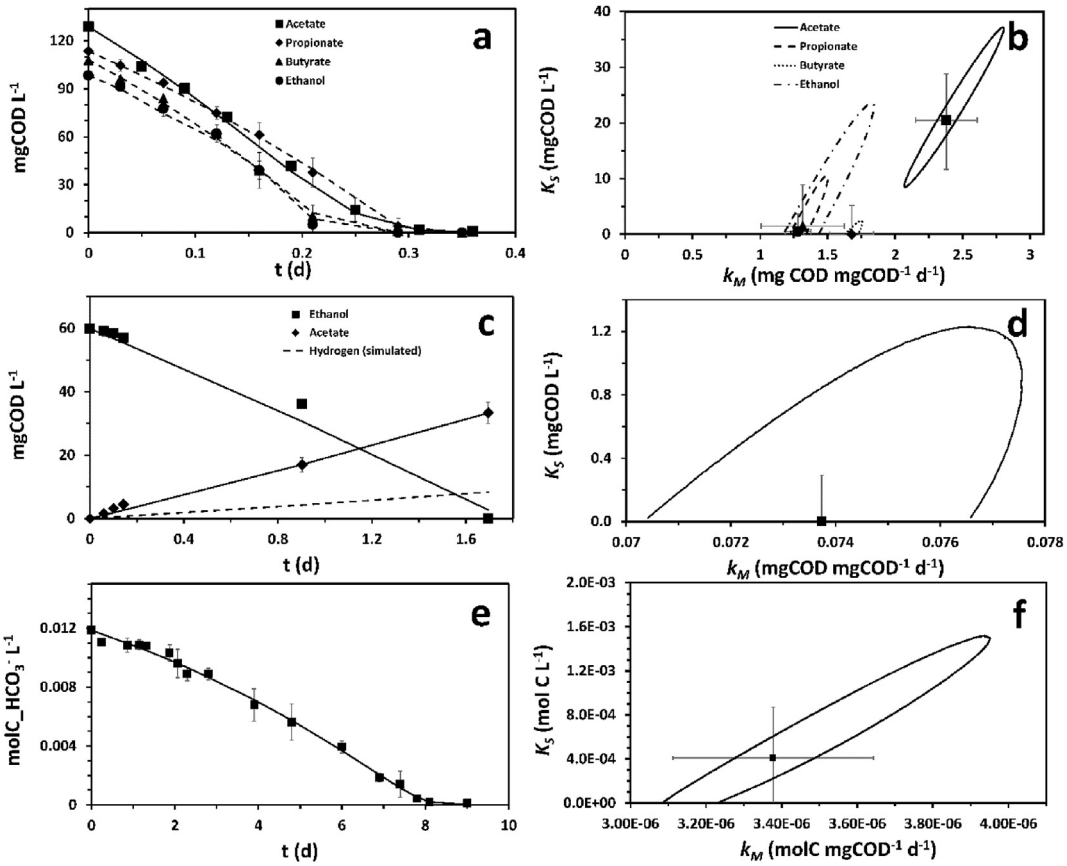

Fig. 2. Experimental (symbols) and modelled (lines) time curse of substrates uptake (left) and parameters determination including 95% confidence intervals and confidence regions (right) of PPB metabolism in photoheterotrophy (a), chemoheterotrophy (b) and photoautotrophy (c) growth modes.

molC^{-1} comparable to the value on acetate (31,560 mgCOD$_{biomass}$ molC^{-1}). However, maximum uptake rate was far lower at $3.4 \pm 0.2 \times 10^{-6}$ molC mgCOD^{-1} d^{-1} (compared to $75 \pm 2 \times 10^{-6}$ molC mgCOD^{-1} d^{-1} on acetate) (Fig. 2f). Photoautotrophy needs to be considered for when there is an excess of bicarbonate and electrons from inorganic sources in the wastewater. It is also important to consider photoautotrophy in order to close mass balances. This case is particularly relevant in light deficiency, where fermentation and anaerobic oxidation processes may become important and hence H_2 is available as a major electron source for PPB.

Nutrient limitation experiments for N and P were used to determine saturation coefficients for N and P. K_S values were extremely low such that the N and P regulation became a switch function (data shown in SI). Biomass assimilated nutrients at a COD/N/P ratio of 100/7.1/1.8, which is higher than conventional aerobic bacteria and much higher than other anaerobes (Tchobanoglous et al., 2002). These values are in line with previous works (Hulsen et al., 2014). However, PPB were able to grow at a lower rate once the nutrients were completely consumed (42% lower than in full nutrient conditions), likely due to fixation of headspace N_2 (Hunter et al., 2008) (inhibited in the presence of ammonium). Nitrogen fixation is completely inhibited at any concentration of ammonium (threshold less than 20 mgN L^{-1}), and the nitrogenase activation requires of a lag phase with no ammonium concentration to be active again (section S5 of SI), likely due to activation of the transcription of nitrogenase genes during static (not growing) conditions (Masepohl et al., 2002). Also, PPB can accumulate polymers such as poly-P (Liang et al., 2010) as well as PHA (Melnicki et al., 2009), which can be used in static growth mode. Since the model developed here is sustained on biomass growth in presence of nitrogenase inhibiting ammonium, nutrient limitation for growth must be included.

3.2. Endogenous processes – hydrolysis and decay

Hydrolysis and decay are considered as transversal first order biochemical processes in most models (Batstone et al., 2006; Henze et al., 2000; Szilveszter et al., 2010). These could be considered separately, since phototrophic growth can be restricted in the absence of irradiance, and decay can be determined directly by

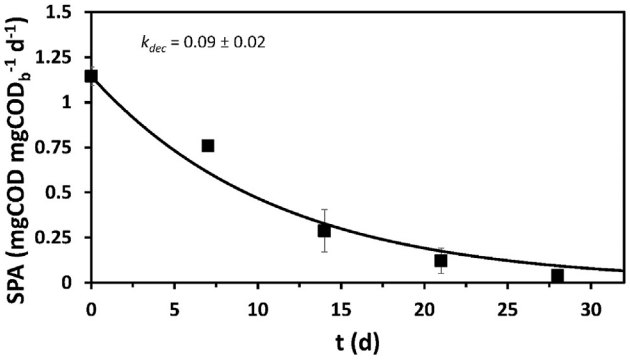

Fig. 3. Mechanism of decay rate. Time course of specific phototrophic activity of PPB subjected to starvation under full illumination.

measurement of phototrophic activity following periods of irradiation without substrate. Fig. 3 shows the time series of the SPA values (on acetate) calculated for the PPB biomass during starvation. Biomass activity reduced according to a first order model with decay coefficient of 0.09 ± 0.02 d^{-1}. Hydrolysis was assessed in dark conditions with substrate present, to avoid re-assimilation of products by PPB. Therefore, hydrolysis products (organic C sources as COD, inorganic C as HCO_3^-, N as NH_4^+ and P as PO_4^{3-}) could be measured and were directly correlated with first order kinetics of the hydrolytic process. Hydrolysis also followed a first order model with a hydrolysis coefficient of 0.071 ± 0.002 d^{-1} (Fig. 4). It should be noted that hydrolysis is substrate specific, and is highly situation specific (Batstone et al., 2015), but that a value of close to 0.1 d^{-1} is comparable with hydrolysis kinetics under anaerobic conditions, but much lower than that for aerobic processes (Henze et al., 2000).

4. Discussion

4.1. Parameter values vs pure culture PPB

A full list of parameter values can be found in the SI, whereas Table 3 shows parameters determined from the literature in comparison with those reported here. Parameters were calculated on the basis that (i) protein composition of PPB is in all cases 60% of dry weight (McKinlay and Harwood, 2010), (ii) 1 g VSS = 1.78 gCOD and (iii) PPB biomass equation is $CH_{1.8}O_{0.38}N_{0.18}$ (McKinlay and Harwood, 2010).

In general, biomass yields calculated here are in line with values reported in the literature (Table 3). The only exception is the biomass yield for autotrophic growth, where no relevant values have been found and only indirect calculation can be performed. Wang et al. (1993) reported biomass growth and CO_2 fixation in *Rhodobacter sphaeroides* and *Rhodospirillum rubrum* using different electron sources (H_2, thiosulfate, sulfide and malate) and the biomass yield values extracted from their activities vary considerably with an average value of 84,000 mgCOD $molC^{-1}$ fixed. These values, however, did not consider re-fixation of CO_2 from malate that may underestimate considerably real CO_2 usage for growth in the Calvin cycle (McKinlay and Harwood, 2011). Therefore the biomass yield differs from the value reported here (36,100 ± 850 mgCOD $molC^{-1}$ fixed). The value determined during this study is however very close to the theoretical maximum yield for carbon dioxide fixation of 39,840 mgCOD $molC^{-1}$, and as such, is a reasonable value.

However, specific uptake rates were substantially different to the literature values depending on the growth mechanism, which may be due to use of pure cultures in contrast with mixed cultures used in the present work. Generally, chemoheterotrophic parameters, pure cultures have an activity close to two orders of magnitude higher than the mixed culture in this work. This results in activities similar to those of typical fermentative bacteria. An example is found in (Schultz and Weaver, 1982) where the growth rates of *Rhodospirillum rubrum* and *Rhodopseudomonas capsulata* were studied on several chemoheterotrophic substrates in the dark. The authors used trimethylamine-N-oxide as accessory electron acceptor on fructose, glucose and succinate, likely removing electron management as a major limitation. Photoheterotrophic parameters also diverged depending on the substrate. While acetate uptake rates were similar to the values reported here (Golomysova et al., 2010; McKinlay and Harwood, 2011), those obtained from other organics, such as malate (Gadhamshetty et al., 2008; Klein et al., 1991), lactate + malate (Obeid et al., 2009), or butyrate (McKinlay and Harwood, 2011) were almost one order of magnitude higher. These parameters were obtained in hydrogen production studies. Under these situations, the substrate uptake is optimized for biogenic H_2 by dislocating catabolism from anabolism due to excess of electrons. This increases considerably the substrate uptake rate while minimizing yield (Basak and Das, 2007). In this work, the μ_{max} for photoheterotrophic metabolism was calculated to be 1.54 d^{-1}, which corresponds to a doubling time of 0.45 d. It is similar to those reported by McKinlay and Harwood (2011) (0.27–0.44 d), and generally aligns well with purple phototrophic bacteria (Hunter et al., 2008). The use of pure cultures promotes specific uptake rates to the detriment of substrate affinity. This leads to increased k_M and K_S parameters, a typical behavior of r-strategist microorganisms (Dorodnikov et al., 2009).

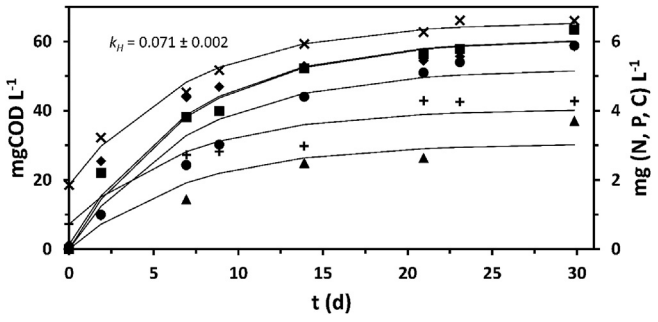

Fig. 4. Time course of released products upon starvation in dark conditions demonstrating hydrolysis: soluble organic compounds but acetate (squares), acetate (diamonds), hydrogen (triangles), TIC (pluses), NH_4^+-N (circles) and PO_4^{3-}-P (crosses).

Hydrolysis and decay rates are commonly substrate specific, with a decrease in rate as redox decreases. In general, for a given material, the hydrolysis coefficient increases from anaerobic to anoxic, and from anoxic to aerobic (Henze et al., 2000). The biomass decay and hydrolysis constants found in literature were obtained in aerobic photoheterotrophic processes (Huang et al., 1999, 2001). This explains considerably higher values than those calculated here.

Compared with previous analyses, this study is focused on mixed culture photoheterotrophic metabolism. The biomass seems to be a K-strategist which promotes substrate affinity over uptake, a microbial strategy in low-strength systems as domestic wastewater with low hydraulic retention times (less than 12 h). Such behavior is useful for out-competing other fast-growing microorganisms. It is clearly effective when compared to the slow growing methanogens, which are the only competitors for acetate under anaerobic conditions with low concentrations of sulfate or oxidized metals (Dorodnikov et al., 2009). Indeed, PPB microorganisms have been demonstrated to prevail and dominate in continuous PAnMBR reactors treating real domestic wastewater without previous inoculation, both in mesophilic (Hülsen et al., 2016b) as well as in psychrophilic (Hülsen et al., 2016a) conditions.

4.2. Model application

The model was tested in a realistic scenario, with influent profile generated using the BSM influent generator (Gernaey et al., 2011). Detailed information about the simulations is provided in the SI.

4.2.1. Fate of C, N and P

The model indicates different SCOD removal efficiencies for particular periods of operation. In general, adaptation to seasonal periods of variable wastewater composition is rapid, as can be shown in input values from Figs. 5 and 6. For periods (I) and (III), which correspond to no additional acetate in the system (average inlet SCOD of 293.1 ± 0.8 mgCOD L^{-1}), the mean SCOD removal efficiency is 81% (Fig. 5a) The remaining SCOD in the system can be

Table 3
Comparison of estimated parameters with those reported in the literature.

Parameter	Units	Estimated values	Literature values	Refs.
$k_{M,ac}$	mgCOD mgCOD^{-1} d^{-1}	2.4	1.5 (0.5), n = 2	(Golomysova et al., 2010; McKinlay and Harwood, 2011)
$k_{M,ph}$	mgCOD mgCOD^{-1} d^{-1}	1.4	11 (13), n = 12	(Gadhamshetty et al., 2008; Golomysova et al., 2010; Klein et al., 1991; McKinlay and Harwood, 2011; Obeid et al., 2009)
$k_{M,ch}$	mgCOD mgCOD^{-1} d^{-1}	0.074	5 (4), n = 8	(Madigan and Gest, 1978; Schultz and Weaver, 1982)
$k_{M,ic}$	molC mgCOD^{-1} d^{-1}	3.4 10^{-6}	2.5 10^{-5} (1.7 10^{-5}), n = 9	(Sarles and Tabita, 1983; Wang et al., 1993)
$K_{S,s}$	mgCOD L^{-1}	0.5	4333 (6036), n = 2	(Gadhamshetty et al., 2008; Obeid et al., 2009)
$Y_{PB,ph}$	mgCOD mgCOD^{-1}	1.1	0.78 (0.37), n = 17	(Gadhamshetty et al., 2008; Klamt et al., 2002; Klein et al., 1991; McKinlay and Harwood, 2011; Obeid et al., 2009; Schultz and Weaver, 1982)
$Y_{PB,ch}$	mgCOD mgCOD^{-1}	0.5	0.23 (0.12), n = 8	(Madigan and Gest, 1978; Schultz and Weaver, 1982)
$Y_{PB,a}$	mgCOD molC^{-1}	36,100	132,000 (84,000), n = 4	(Wang et al., 1993)
k_{hyd}	d^{-1}	0.07	0.27 (0.06), n = 2	(Huang et al., 1999, Huang et al. 2001)
k_{dec}	d^{-1}	0.09	0.2 (0.02), n = 2	(Huang et al., 1999, Huang et al. 2001)

mainly attributed to the presence of non-biodegradable SCOD, accounting for 71% of the effluent SCOD. During period (II) acetate was added to agree with the COD/N/P requirements for PPB. Average SCOD removal efficiency slightly increased up to around 85% due to optimized COD/N/P conditions. As in the Stage I, the major part of the remaining SCOD corresponded to soluble inerts. The model, however, is not able to reproduce the PPB behavior under a high excess of inlet SCOD concentration since it is based on assimilative mechanisms only and accumulation processes are not included, as e.g. PHA or glycogen. The PPB biomass is able to accumulate these compounds (Brandl et al., 1991; Melnicki et al., 2009), and so SCOD removal efficiencies are expected to be higher and less dependent on nutrients in real cases (Hülsen et al., 2016a, 2016b). An upgraded model including accumulative mechanisms is therefore needed for high COD:N ratio wastewater. However, this model is suitable for normal DWW treatment operation, where N and P are generally in excess.

Nutrient assimilation was directly linked with biomass growth. The optimum assimilative COD/N/P relationship has been calculated to be 100/7.1/1.8 from batch experiments. Therefore, periods with non-optimal ratios are expected to have higher effluent nutrient concentrations. Under normal situation (periods (I) and (III)), with no additional acetate, nutrients were not completely removed and ammonium and phosphate efficiencies were 45% and 56%, respectively (Fig. 5b and c, respectively), averaging effluent concentrations of 23 mgN L^{-1} and 2.5 mgP L^{-1}, respectively. This justifies the need for extra SCOD addition, as has been previously described experimentally (Hülsen et al., 2016b). Phosphorus was almost completely removed during C and N sufficiency during period (II), with removal efficiencies of 89% (effluent concentrations of 0.5 mgP L^{-1}). However, depletion of P prevented a high N removal due to nutrient imbalance, and so N removal efficiencies during these periods averaged 70%, averaging effluent concentrations of 11 mgN L^{-1}. Again, accumulative mechanisms may have a key role here, as PPB are able to accumulate poly-P (Liang et al., 2010). This mechanism is quite complex and has not been properly defined, particularly in mixed cultures and on wastewater sources.

Production of biomass was related to PPB growth as well as input solids. Biomass fractionation (X_{PB}, X_S and X_I) along the simulation period is depicted in Fig. 6. When acetate was not added, PPB biomass was produced at 26.9% of the total biomass in the outlet (sludge line). Adding acetate increased this value up to 34.9% of total biomass. Accumulation of X_S within the reactor is a direct consequence of low hydrolysis coefficient in combination with short SRT. Additional substrate increased biomass concentration due to assimilation of the remaining N and P. This also boosted the SRT, and decay was more prominent, increasing X_S concentrations up to values above 1000 mgCOD L^{-1} (see stage (II) in Fig. 6). Inerts fraction, however, was always below 32% of the total particulates concentration, probably due to the slow hydrolysis rate. These results have an important effect on energy distribution in the PRR platform since all energy balances are directly related with the biomass management through anaerobic digestion, and the relative amount of PPB will influence potential anaerobic degradability and biomass consistency. An important aspect identified by this continuous analysis is that the biomass fraction X_{PB} is always relatively small, even when applying a settler (compared with activated sludge streams predicted by the ASM1). This is because the hydrolysis coefficient is very low (<0.1 d^{-1}) compared with the levels of >2 d^{-1} typically applied in the ASM1, ASM2 and ASM2d (Henze et al., 2000). This means that while growth rates are comparable to activated sludge, hydrolysis rates are far lower, and hence metabolic activity is dominated by available soluble substrate (and possibly N and P) rather than electron acceptor availability. In any case, there will always be a large proportion of undegraded particulates, due to the slow hydrolysis coefficient, and in a stable, solids dominated system, PPB sludge should be more analogous to primary sludge rather than activated sludge, with both negative and positive consequences.

pH followed some important general trends. During normal operation, it varied 6.5–7.5, according to the VFA and bicarbonate uptake cycles. The overall pH was largely regulated by the presence of bicarbonate, in opposition with inorganic nitrogen (S_{IN}). However, in specific periods where the influent had bicarbonate limitations (approximately 2–3 weeks every 6 months), where bicarbonate was completely depleted, pH could rise to 8.5–9 due to the unbalanced presence of ammonia and cations. This was attenuated in the simulation where cations were linked to bicarbonate, but was still a factor. We have seen batch tests rise to pH 9 with no substantial impact on activity, and it is less evident, but obviously still important in continuous operation. Very low pH levels (<6.0) never occurred, due to the lack of nitrification. Likewise, at the ammonia levels present, despite the high pH, free ammonia inhibition was never a risk, though it would be more important in industrial wastewaters.

Simulation of biomass behavior has implications on biomass production upon main line biological treatment. There is a net

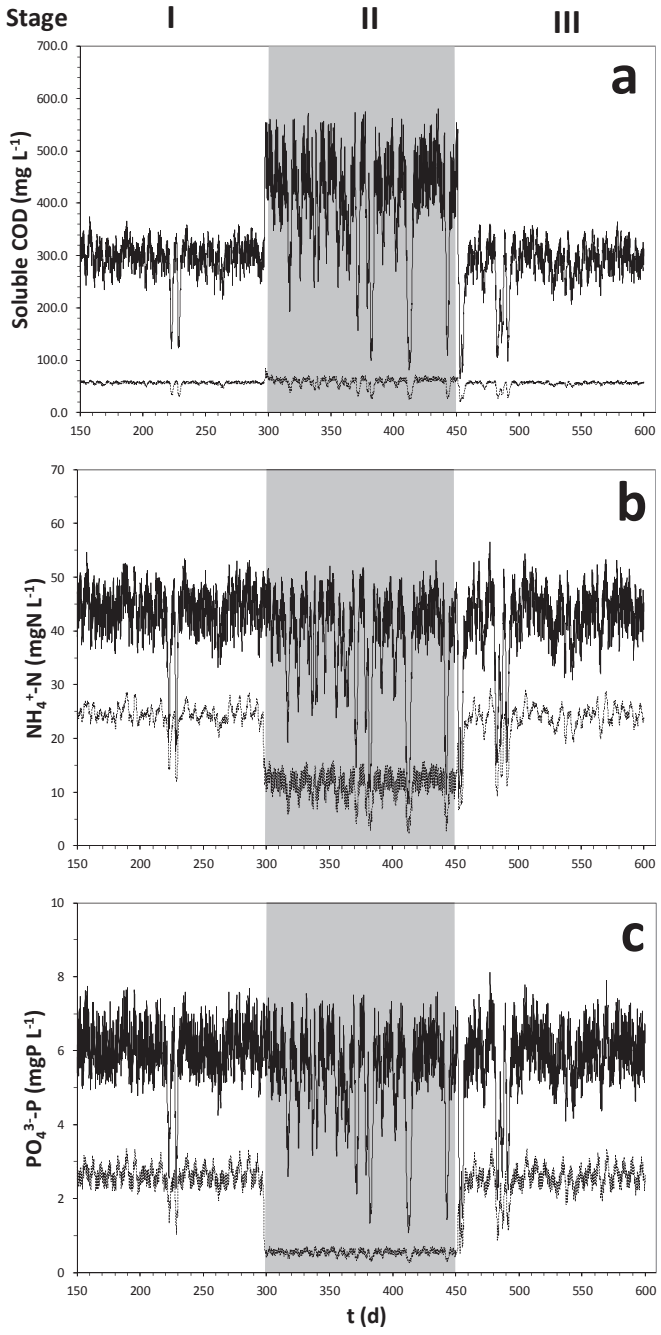

Fig. 5. Influent (continuous line) and effluent concentrations (dash line) over time for PAnMBR simulation for SCOD (a), ammonium (b) and phosphate (c) upon primary settling. Different operational periods are indicated as vertical shades separators.

increment of biomass production yield compared to typical activated sludge processes. This could have an impact in energy recovery (through biogas) but also in sludge waste disposal expenses, which can be partially counteracted by downstream production of high value-added bioresources as proteins, prebiotics and probiotics (Matassa et al., 2015) or bioplastics (Padovani et al., 2016), as well as energetic resources as third generation liquid biofuels (Castro et al., 2016).

5. Conclusions

Anaerobic phototrophic growth in domestic wastewater

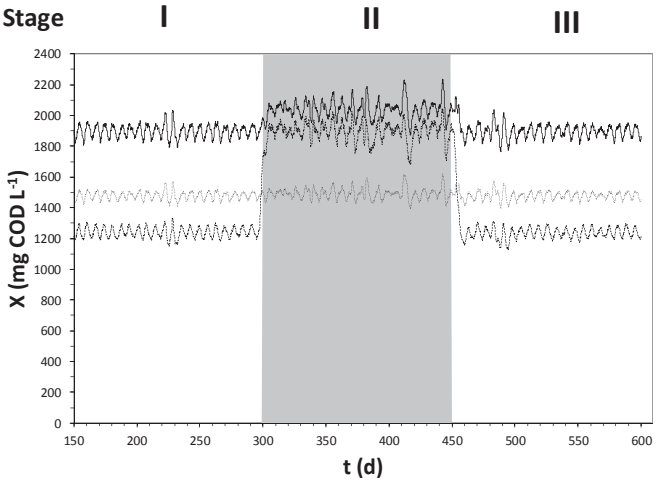

Fig. 6. Biomass fractionation including active phototrophic bacteria (dash line), biodegradable particulate biomass (continuous line) and inert particulate (dot lines) over time for the PAnMBR continuous simulation. Different operational periods are indicated as vertical shades separators.

treatment is fast, comparable to activated sludge (in k_M values) with very low K_S values, indicating that purple phototrophic bacteria behave as K strategist. However, hydrolysis is relatively slow (~0.1 d^{-1}), which means that particulate substrates will not be degraded at short HRTs. The predominant mechanism is photoheterotrophy, with autotrophy and chemotrophy generally slow. The decay rate is relatively high, comparable to activated sludge under aerobic conditions. The dynamics under continuous conditions indicate that biological processes are adaptable to normal flow variations such that performance at a given mode is stable.

The model has the following limitations:

(i) The model is only valid for anaerobic conditions, and hydrogen production for redox balancing is assumed to be inhibited, so this model cannot be implemented for hydrogen production systems as it is.
(ii) Poly-P and other polymers accumulation is not included due to a lack of foundational research. Also, nitrogen fixation is not included since it is assumed to be inhibited by ammonium.

A key priority for future research should be inclusion of poly-P and PHA accumulation as well as N_2 fixation and side H_2 production, as these processes (poly-P without carbon, PHA without oxidation or organics, and N_2/H_2 production) are unique to photoanaerobic organisms. The topic of infrared light delivery has not been addressed in detail in this model, and is generally assumed to be in excess (i.e., not limiting catabolic rate, such that there is no mixed photo-dark fermentation (mixotrophic growth). This could be incorporated by limiting light to enable mixotrophic growth through the existing switch function that considers also spatial separation to dark zones, but as stated above, further work is required to consider accumulation and depletion of storage compounds. This requires a very different approach to (for example, Algae) (reviewed in Béchet et al., 2013) where a more complex model is commonly applied: (considering separately excited, resting, inhibited differential states). We have kept PPB biomass as a single state, with different processes acting on it, which are in turn linked to the presence or absence of irradiance, which would enable more simple extension to energy storage and depletion. This would enable more precise determination of the switch between

stored dark heterotrophic growth and methanogenesis.

Acknowledgements

This work was jointly funded by the Smart Water Fund (project 10OS-023) and the CRC for Water Sensitive Cities (project C2.1). Thanks are given to Prof. James B. McKinlay for his kind discussion on PPB metabolism.

Appendix A. Supplementary data

Supplementary data related to this article can be found at http://dx.doi.org/10.1016/j.watres.2017.03.022.

References

APHA, 1998. Standard Methods for the Examination of Water and Wastewater, twentieth ed. American Public Health Association, Washington, DC, USA.

Basak, N., Das, D., 2007. The prospect of purple non-sulfur (PNS) photosynthetic bacteria for hydrogen production: the present state of the art. World J. Microbiol. Biotechnol. 23 (1), 31–42.

Batstone, D.J., Amerlinck, Y., Ekama, G., Goel, R., Grau, P., Johnson, B., Kaya, I., Steyer, J.P., Tait, S., Takaćs, I., Vanrolleghem, P.A., Brouckaert, C.J., Volcke, E., 2012. Towards a generalized physicochemical framework. Water Sci. Technol. 66 (6), 1147–1161.

Batstone, D.J., Keller, J., Angelidaki, I., Kalyuzhnyi, S., Pavlostathis, S., Rozzi, A., Sanders, W., Siegrist, H., Vavilin, V., 2002. The IWA anaerobic digestion model No 1(ADM 1). Water Sci. Technol. 45 (10), 65–73.

Batstone, D.J., Keller, J., Steyer, J., 2006. A review of ADM 1 extensions, applications, and analysis: 2002-2005. Water Sci. Technol. 54 (4), 1–10.

Batstone, D.J., Pind, P.F., Angelidaki, I., 2003. Kinetics of thermophilic, anaerobic oxidation of straight and branched chain butyrate and valerate. Biotechnol. Bioeng. 84 (2), 195–204.

Batstone, D.J., Puyol, D., Flores-Alsina, X., Rodríguez, J., 2015. Mathematical modelling of anaerobic digestion processes: applications and future needs. Rev. Environ. Sci. Bio/Technol. 14 (4), 595–613.

Brandl, H., Gross, R.A., Lenz, R.W., Lloyd, R., Fuller, R.C., 1991. The accumulation of poly(3-hydroxyalkanoates) in *Rhodobacter sphaeroides*. Arch. Microbiol. 155 (4), 337–340.

Béchet, Q., Shilton, A., Guieysse, B., 2013. Modeling the effects of light and temperature on algae growth: state of the art and critical assessment for productivity prediction during outdoor cultivation. Biotechnol. Adv. 31 (8), 1648–1663.

Castro, A.R., Rocha, I., Alves, M.M., Pereira, M.A., 2016. *Rhodococcus opacus* B4: a promising bacterium for production of biofuels and biobased chemicals. AMB Express 6, 35.

Chen, Y., Cheng, J.J., Creamer, K.S., 2008. Inhibition of anaerobic digestion process: a review. Bioresour. Technol. 99 (10), 4044–4064.

Copp, J.B., Jeppsson, U., Rosen, C., 2003. Towards an ASM1 – ADM1 state variable interface for plant-wide wastewater treatment modeling. In: Proceedings of the 76th Annual WEF Conference and Exposition (WEFTEC). Oct. 11–15, Los Angeles, USA.

Dorodnikov, M., Blagodatskaya, E., Blagodatsky, S., Fangmeier, A., Kuzyakov, Y., 2009. Stimulation of r- vs. K-selected microorganisms by elevated atmospheric CO_2 depends on soil aggregate size: research article. FEMS Microbiol. Ecol. 69 (1), 43–52.

Eroglu, I., 2008. Hydrogen production by *Rhodobacter sphaeroides* O.U.001 in a flat plate solar bioreactor. Int. J. Hydrogen Energy 33 (2), 531–541.

Fang, H.H.P., Liu, H., Zhang, T., 2005. Phototrophic hydrogen production from acetate and butyrate in wastewater. Int. J. Hydrogen Energy 30 (7), 785–793.

Finneran, K.T., Johnsen, C.V., Lovley, D.R., 2003. *Rhodoferax ferrireducens* sp. nov., a psychrotolerant, facultatively anaerobic bacterium that oxidizes acetate with the reduction of Fe(III). Int. J. Syst. Evol. Microbiol. 53 (3), 669–673.

Gadhamshetty, V., Sukumaran, A., Nirmalakhandan, N., Theinmyint, M., 2008. Photofermentation of malate for biohydrogen production— a modeling approach. Int. J. Hydrogen Energy 33 (9), 2138–2146.

Gernaey, K.V., Flores-Alsina, X., Rosen, C., Benedetti, L., Jeppsson, U., 2011. Dynamic influent pollutant disturbance scenario generation using a phenomenological modelling approach. Environ. Model. Softw. 26 (11), 1255–1267.

Golomysova, A., Gomelsky, M., Ivanov, P.S., 2010. Flux balance analysis of photoheterotrophic growth of purple nonsulfur bacteria relevant to biohydrogen production. Int. J. Hydrogen Energy 35 (23), 12751–12760.

Gordon, G.C., McKinlay, J.B., 2014. Calvin cycle mutants of photoheterotrophic purple nonsulfur bacteria fail to grow due to an electron imbalance rather than toxic metabolite accumulation. J. Bacteriol. 196 (6), 1231–1237.

Henze, M., Gujer, W., Mino, T., Van Loosdrecht, M., 2000. Activated Sludge Models ASM1, ASM2, ASM2d and ASM3, vol. 9. IWA Publishing, UK.

Hiraishi, A., Yanase, A., Kitamura, H., 1991. Polyphosphate accumulation by *Rhodobacter sphaeroides* grown under different environmental conditions with special emphasis on the effect of external phosphate concentrations. Bull. Jpn. Soc. Microb. Ecol. 6 (1), 25–32.

Huang, J.S., Jih, C.G., Sung, T.J., 1999. Performance enhancement of suspended-growth reactors with phototrophs. J. Environ. Eng. 125 (6), 501–507.

Huang, J.S., Wu, C.S., Jih, C.G., Chen, C.T., 2001. Effect of addition of *Rhodobacter* sp. to activated-sludge reactors treating piggery wastewater. Water Res. 35 (16), 3867–3875.

Hülsen, T., Barry, E.M., Lu, Y., Puyol, D., Batstone, D.J., 2016a. Low temperature treatment of domestic wastewater by purple phototrophic bacteria: performance, activity, and community. Water Res. 100, 537–545.

Hülsen, T., Barry, E.M., Lu, Y., Puyol, D., Keller, J., Batstone, D.J., 2016b. Domestic wastewater treatment with purple phototrophic bacteria using a novel continuous photo anaerobic membrane bioreactor. Water Res. 100, 486–495.

Hulsen, T., Batstone, D.J., Keller, J., 2014. Phototrophic bacteria for nutrient recovery from domestic wastewater. Water Res. 50, 18–26.

Hunter, C.N., Daldal, F., Thurnauer, M.C., Beatty, J.T., 2008. The Purple Phototrophic Bacteria. Springer, The Netherlands.

Jetten, M.S.M., Horn, S.J., van Loosdrecht, M.C.M., 1997. Towards a more sustainable municipal wastewater treatment system. Water Sci. Technol. 35 (9), 171–180.

Kantachote, D., Torpee, S., Umsakul, K., 2005. The potential use of anoxygenic phototrophic bacteria for treating latex rubber sheet wastewater. Electron. J. Biotechnol. 8 (3), 314–323.

Kim, M.K., Choi, K.-M., Yin, C.-R., Lee, K.-Y., Im, W.-T., Lim, J.H., Lee, S.-T., 2004. Odorous swine wastewater treatment by purple non-sulfur bacteria, *Rhodopseudomonas palustris*, isolated from eutrophicated ponds. Biotechnol. Lett. 26 (10), 819–822.

Klamt, S., Schuster, S., Gilles, E.D., 2002. Calculability analysis in underdetermined metabolic networks illustrated by a model of the central metabolism in purple nonsulfur bacteria. Biotechnol. Bioeng. 77 (7), 734–751.

Klein, G., Klipp, W., Jahn, A., Steinborn, B., Oelze, J., 1991. The relationship of biomass, polysaccharide and H_2 formation in the wild-type and nifA/nifB mutants of *Rhodobacter capsulatus*. Arch. Microbiol. 155 (5), 477–482.

Lee, H.-S., Vermaas, W.F., Rittmann, B.E., 2010. Biological hydrogen production: prospects and challenges. Trends Biotechnol. 28 (5), 262–271.

Liang, C.-M., Hung, C.-H., Hsu, S.-C., Yeh, I.-C., 2010. Purple nonsulfur bacteria diversity in activated sludge and its potential phosphorus-accumulating ability under different cultivation conditions. Appl. Microbiol. Biotechnol. 86 (2), 709–719.

Madigan, M.T., Gest, H., 1978. Growth of a photosynthetic bacterium anaerobically in darkness, supported by "oxidant-dependent" sugar fermentation. Arch. Microbiol. 117 (2), 119–122.

Masepohl, B., Drepper, T., Paschen, A., Groß, S., Pawlowski, A., Raabe, K., Klipp, W., 2002. Regulation of nitrogen fixation in the phototrophic purple bacterium Rhodobacter capsulatus. J. Mol. Microbiol. Biotechnol. 4 (3), 243–248.

Matassa, S., Batstone, D.J., Hülsen, T., Schnoor, J., Verstraete, W., 2015. Can direct conversion of used nitrogen to new feed and protein help feed the world? Environ. Sci. Technol. 49 (9), 5247–5254.

McKinlay, J.B., Harwood, C.S., 2010. Carbon dioxide fixation as a central redox cofactor recycling mechanism in bacteria. Proc. Natl. Acad. Sci. U. S. A. 107 (26), 11669–11675.

McKinlay, J.B., Harwood, C.S., 2011. Calvin cycle flux, pathway constraints, and substrate oxidation state together determine the H_2 biofuel yield in photoheterotrophic bacteria. MBio 2 (2) e00323–00310.

Melnicki, M.R., Eroglu, E., Melis, A., 2009. Changes in hydrogen production and polymer accumulation upon sulfur-deprivation in purple photosynthetic bacteria. Int. J. Hydrogen Energy 34 (15), 6157–6170.

Muñoz, R., Guieysse, B., 2006. Algal–bacterial processes for the treatment of hazardous contaminants: a review. Water Res. 40 (15), 2799–2815.

Nopens, I., Batstone, D.J., Copp, J.B., Jeppsson, U., Volcke, E., Alex, J., Vanrolleghem, P.A., 2009. An ASM/ADM model interface for dynamic plant-wide simulation. Water Res. 43 (7), 1913–1923.

Obeid, J., Magnin, J., Flaus, J., Adrot, O., Willison, J., Zlatev, R., 2009. Modelling of hydrogen production in batch cultures of the photosynthetic bacterium *Rhodobacter capsulatus*. Int. J. Hydrogen Energy 34 (1), 180–185.

Overmann, J., Garcia-Pichel, F., 1998. In: Dworkin, M. (Ed.), The Phototrophic Way of Life: the Prokaryotes: an Evolving Electronic Resource for the Microbiological Community. Springer, New York (The Netherlands).

Padovani, G., Carlozzi, P., Seggiani, M., Cinelli, P., Vitolo, S., Lazzeri, A., 2016. PHB-rich biomass and BioH2 production by means of photosynthetic microorganisms. Chem. Eng. Trans. 49, 55–60.

Patton, C.J., Truitt, E.P., 1992. Methods of Analysis by the US Geological Survey National Water Quality Laboratory: Determination of the Total Phosphorus by a Kjeldahl Digestion Method and an Automated Colorimetric Finish that Includes Dialysis. Open-File Report 92–146. US Geological Survey, USA.

Rodionov, Y.V., Lebedeva, N.V., Kondratieva, E.N., 1986. Ammonia inhibition of nitrogenase activity in purple and green bacteria. Arch. Microbiol. 143 (4), 345–347.

Sarles, L.S., Tabita, F.R., 1983. Derepression of the synthesis of D-ribulose 1, 5-bisphosphate carboxylase/oxygenase from *Rhodospirillum rubrum*. J. Bacteriol. 153 (1), 458–464.

Schultz, J., Weaver, P., 1982. Fermentation and anaerobic respiration by Rhodospirillum rubrum and *Rhodopseudomonas capsulata*. J. Bacteriol. 149 (1), 181–190.

Szilveszter, S., Ráduly, B., Ábrahám, B., Lányi, S., Niculae, D.R., 2010. Mathematical models for domestic biological wastewater treatment process. Environ. Eng. Manag. J. 9 (5), 629–636.

Tait, S., Tamis, J., Edgerton, B., Batstone, D.J., 2009. Anaerobic digestion of spent

bedding from deep litter piggery housing. Bioresour. Technol. 100 (7), 2210–2218.
Tao, Y., He, Y., Wu, Y., Liu, F., Li, X., Zong, W., Zhou, Z., 2008. Characteristics of a new photosynthetic bacterial strain for hydrogen production and its application in wastewater treatment. Int. J. Hydrogen Energy 33 (3), 963–973.
Tchobanoglous, G., Stensel, H.D., Tsuchihashi, R., Burton, F.L., 2002. Wastewater Engineering: Treatment and Reuse, Metcalf and Eddy Inc, fourth ed. McGraw-Hill Education, New York, NY, USA.
Uyar, B., Eroglu, I., Yücel, M., Gündüz, U., Türker, L., 2007. Effect of light intensity, wavelength and illumination protocol on hydrogen production in photo-bioreactors. Int. J. Hydrogen Energy 32 (18), 4670–4677.
Wang, X., Modak, H.V., Tabita, F.R., 1993. Photolithoautotrophic growth and control of CO_2 fixation in *Rhodobacter sphaeroides* and *Rhodospirillum rubrum* in the absence of ribulose bisphosphate carboxylase-oxygenase. J. Bacteriol. 175 (21), 7109–7114.
Yetis, M., Gündüz, U., Eroglu, I., Yücel, M., Türker, L., 2000. Photoproduction of hydrogen from sugar refinery wastewater by *Rhodobacter sphaeroides* OU 001. Int. J. Hydrogen Energy 25 (11), 1035–1041.
Zhu, H., Suzuki, T., Tsygankov, A.A., Asada, Y., Miyake, J., 1999. Hydrogen production from tofu wastewater by *Rhodobacter sphaeroides* immobilized in agar gels. Int. J. Hydrogen Energy 24 (4), 305–310.